Review

Photoacoustic Imaging of Human Skin for Accurate Diagnosis and Treatment Guidance

Yue Ying , Hong Zhang * , Li Lin *

Posted Date: 23 January 2024

doi: 10.20944/preprints202401.1651.v1

Keywords: photoacoustic imaging; skin cancer; psoriasis; diagnosis; treatment guidance

Review

Photoacoustic Imaging of Human Skin for Accurate Diagnosis and Treatment Guidance

Yue Ying [1], Hong Zhang [1,3,*] and Li Lin [1,2,*]

[1] College of Biomedical Engineering and Instrument Science, Zhejiang University, Hangzhou, China.
[2] The First Affiliated Hospital, Zhejiang University School of Medicine, Hangzhou, China.
[3] The Second Affiliated Hospital, Zhejiang University School of Medicine, Hangzhou, China.
* Correspondence: Email: hzhang21@zju.edu.cn, linliokok@zju.edu.cn

Abstract: Photoacoustic imaging (PAI) is a cutting-edge biomedical imaging modality, providing detailed anatomical and functional information about the area beneath the skin surface. Its light energy deposition is such that PAI typically provides clear images of the skin with high signal-to-noise ratios. Specifically, the rich optical contrast of PAI allows biological information related to lesion growth, malignancy, treatment response, and prognosis to be seen. Given its significant advantages and emerging role in imaging skin lesions, we summarize and comment on representative studies of skin PAI, such as the guidance of skin cancer biopsies and surgical excisions, and the accurate diagnosis of psoriasis. We conclude with our insights about the clinical significance of skin PAI, showing how its use to identify biological characteristics in lesion microenvironments allows early diagnosis and prognosis of disease.

Keywords: photoacoustic imaging; skin cancer; psoriasis; diagnosis; treatment guidance

1. Introduction

Skin diseases are complex and widespread. They include inflammatory, infectious, autoimmune, neoplastic, and genetic skin diseases with different origins, symptoms, and severity. As a consequence, accurate diagnosis is essential to achieve effective treatment with appropriate patient management. Misdiagnosis may lead to ineffective therapy, unnecessary side effects, or erroneous treatment. Accordingly, a high-resolution, informative, and safe imaging modality is preferred to provide accurate diagnosis and treatment feedback for improved patient management[1].

Accurate skin disease diagnosis and treatment assessment require sensitive imaging of the lesion's anatomical and pathological information with high spatiotemporal resolution. Multiple imaging modalities have been developed for such goals, including dermoscopy[2,3], reflectance confocal microscopy[4,5], optical coherence tomography (OCT)[6,7], and ultrasonography[8,9]. In general, optical microscopy provides high spatial resolutions but is unable to focus under the epidermis beyond the ballistic regime of light (~1 mm)[10,11]. Ultrasonography penetrates deeper but is often limited to morphological information without insight into the pathological environment[12]. Each imaging technique has certain advantages and limitations. Skin imaging therefore requires a modality complementary to these existing techniques, to bridge between the microscopic and macroscopic scales with rich optical contrast.

Photoacoustic imaging (PAI), also known as optoacoustic imaging, is a biomedical imaging modality that combines optical excitation and acoustic detection and which shows promise for fulfilling the above requirements. PAI has been demonstrated to provide a scalable field of view (FOV), high spatiotemporal resolutions, and pathology-related imaging contrast without ionizing radiation or contrast agent injection. It uses a pulsed laser to irradiate biological tissues. The absorbed photons heat the biological chromophores instantaneously and generate a rise in pressure by transient thermoelastic expansion. The pressure rise then propagates outward in the form of

 doi:10.20944/preprints202401.1651.v1

ultrasonic waves (photoacoustic waves), which suffer negligible scattering before being detected by ultrasonic transducers placed around the tissue. The amplitude of the pressure rise can then be calculated via image reconstruction algorithms, revealing the concentration and distribution of the chromophores beneath the skin surface[13–15]. The optical absorption-based contrast and the hybrid nature of PAI enables the acquisition of structural, functional, and molecular information with a high depth-to-resolution ratio[16–18].

In PAI, the high optical contrast permits analysis of pathological characteristics with or without labeling, the high depth-to-resolution ratio allows clear visualization of detailed features from the epidermis to the dermis, and the high imaging speed reduces motion artifacts and facilitates fast scanning. PAI therefore shows early promise for accurate diagnosis and treatment guidance of various skin diseases with improved patient management. In this review, we first introduce the major configurations of PAI and then present multiple applications of PAI in dermatology with clinical translation potentials. We conclude with a summary and outlook on this field, aiming to illustrate the unique role of PAI in solving critical problems in the diagnosis and treatment of skin cancer and psoriasis, as well as other skin diseases.

2.Key Features of PAI

Most PAI systems can be classified into three categories according to their image formation approach: optical-resolution photoacoustic microscopy (OR-PAM), acoustic-resolution photoacoustic mesoscopy (AR-PAM), and photoacoustic computed tomography (PACT). Specifically, OR-PAM relies on rapid scanning of a tightly focused light beam to render optical-resolution images near the surface[19–21]. In comparison, AR-PAM scans a loosely focused light beam for excitation but a focused ultrasound beam for detection[22,23]. In AR-PAM, the acoustic focus typically generates coarser lateral resolutions than the optical focus in OR-PAM, but generally images deeper than OR-PAM since ultrasound scatters much less than light in biological tissues[24]. For even deeper penetration, PACT usually uses expanded light beams to excite the tissue homogenously and detects PA waves using multiple ultrasonic transducers in parallel[25,26]. Consequently, the images are reconstructed via acoustic inversion algorithms in the optical diffusive regime. All three PAI configurations make PAI scalable from epidermis to dermis with a high depth-to-resolution ratio (~200), thus bridging the longstanding gap between microscopic and macroscopic observations of skin (Table 1).

Table 1. Key features of the major configurations of PAI.

	OR-PAM	AR-PAM	PACT
Depth	<1.5mm[19–21]	≤5mm[22,23]	≤40mm[13]
Penetrated skin layers	Epidermis and partially dermis	Epidermis, dermis, and subcutaneous tissue	Epidermis, dermis, and subcutaneous tissue
Resolution	Lateral: 0.3–5 μm Axial: 15–30 μm[27,28]	Lateral: 20–80 μm Axial: 20–60 μm[29]	30–400 μm[13,26]
Resolved features	Capillaries	Arterioles and venules	Arterioles, venules, and larger vessels
Frame rate	a few hertz[21,27,30]	several tens of hertz[22,23]	several tens or even hundreds of hertz[13,26]

The distinct absorption spectra of biological components allow PAI to reveal comprehensive information about the lesion. By scanning the excitation light through multiple wavelengths, PAI can image a variety of endogenous or exogenous absorbers, enabling the detection of anatomical,

 doi:10.20944/preprints202401.1651.v1

physiological, metabolic, molecular, and genetic events in the body. The abundant imaging information allows PAI to detect the presence of specific biomolecules and pathological features, identifying the lesion's malignancy and progression[26,31–33]. The diagnostic capability of PAI can be further extended to the guidance of treatment and assessment of therapy, facilitating accurate and personalized treatment to treat skin cancer and psoriasis, as well as other skin diseases.

High imaging speed is critical for imaging living objects or dynamic biological processes. PAI can acquire images up to hundreds of frames per second, reducing motion-induced artifacts and improving imaging efficiency. For example, PAI can scan a whole human breast within a single breath hold of 10 seconds[13]. Thus, high imaging speed is one of the significant advantages of PAI, enabling real-time monitoring of biological processes in vivo.

3. Clinical Applications in Skin Imaging

Here, we focus on PAI of the skin and present its studies aiming at fulfilling the clinical requirements in the diagnosis and treatment of skin cancer and psoriasis, among numerous skin diseases. For skin cancer diagnosis and treatment assessment, there has been significant research on precise measurements of tumor thickness as well as blood vasculatures and oxygenation states in the tumor microenvironment. Other than imaging solid tumors, PAI can detect circulating tumor cells, providing early promise in treatment assessment and prognosis. In addition to cancer imaging, PAI studies have paid special attention to psoriasis diagnosis, offering precise and objective evaluations.

3.1. Skin Cancer Imaging

3.1.1. PAI of Melanoma

Normal human skin is divided into three layers: epidermis, dermis, and subcutaneous tissue (Figure 1(a)). Melanocytes, located in the basal layer of the epidermis, are normal human cells which produce pigment and protect the skin from ultraviolet radiation. Melanoma, which is the deadliest form of skin cancer, arises from the malignant transformation of melanocytes[34]. Although it accounts for only 5% of skin cancers, melanoma is responsible for over 60% of skin cancer-related deaths[35–37].

Tumor thickness is an important indicator of melanoma progression and metastasis. Melanoma cells initially grow within the epidermis layer, in what is usually called the "horizontal growth phase". Accurate diagnosis followed by extended surgical resection at this stage would remove tumor cells with minimal risk of recurrence. Without proper treatment, however, tumor cells will start to invade the dermis during the "vertical growth phase". Blood and lymph vessels distributed in the dermis will facilitate melanoma cell metastasis, which may lead to fatality. Accordingly, tumor thickness is a key factor in staging melanoma, guiding treatment and assessing prognosis[35,38].

Accurate measurement of melanoma thickness remains a challenge in clinics due to the limited imaging depth of skin imagers and the low imaging contrast to reveal the lesions' pathological features. Currently, surgical excision biopsy with narrow margins and partial biopsy are typically applied for this purpose[39,40]. Although dermatology guidelines recommend biopsy from the irregular and hyperpigmented sections, insufficient sampling of the primary lesion limits the accuracy of partial biopsy[41]. Consequently, a comprehensive and precise measurement of melanin distribution and the melanoma microenvironment can improve early diagnosis and guidance in deciding the positions and depths of biopsies.

The high optical contrast allows PAI to reveal the melanin content in melanoma cells beneath the epidermis. For example, Breathnach et al. developed a handheld PAI probe to measure melanoma thickness (Figure 1(b))[42]. While the thickness of the lesions measured by PACT was highly correlated with histology ($r = 0.99$, $P < 0.001$ for melanoma, $r = 0.98$, $P < 0.001$ for nevi), the limited view of the linear ultrasonic array compromised the image clarity. Another linear array-based PACT system was used for melanoma measurement at depths ranging from 0.2 to 6.0 mm[43]. Probably due to the dehydration and shrinkage of histology samples, the system quantified slightly thicker (around 13% thicker) tumor depth in vivo compared to histological measurements ex vivo[42,43]. The

 doi:10.20944/preprints202401.1651.v1

distinctive oxy-hemoglobin (HbO_2) and deoxy-hemoglobin (HbR) signals captured by PACT revealed vascular infiltration surrounding melanin-rich areas, providing additional features to diagnose the tumor's invasiveness[22,44–48] (Figure 1(c)).

In addition to the depth, blood vasculatures in the melanoma's microenvironment are closely associated with the invasiveness and metastatic stages of the tumor. Accordingly, three-dimensional imaging of the vascular features across the skin layers can provide pathological details around the tumor which are inaccessible via traditional dermatoscopy. He et al. imaged microvessels throughout the skin to a depth of 1.5 mm at a wavelength of 532 nm within a single breath hold of 15 seconds, with a resolution of tens of micrometers (Figure 1(d))[46]. In vivo images from 10 melanoma and 10 benign moles showed significant difference in microvasculatures (e.g., the dermal vasculature in the melanoma edge areas exhibited a significantly higher total blood volume and vessel density compared to the melanocytic nevus) between malignant and benign lesions, showing early promise for diagnostic improvement.

Multiple PAI studies have demonstrated measurement of melanoma depths with verified histopathological correlation. In addition, clear imaging of the hemogenous characteristics further faciliate the non-invasive assessement of the lesion's malignancy and invasiveness. Therefore, preoperative PAI of melanoma can be a useful tool for biopsy guidance, allowing more accurate sampling and eliminating the need for redundant biopsies.

3.1.2. Detection and Treatment of Circulating Melanoma Cells

Circulating melanoma cells (CMCs), an exclusive subset of circulating tumor cells[49], are melanoma cells that have detached from the tumor and circulated in the bloodstream. Since CMCs are critical indicators of tumor metastasis[50,51], the identification and quantification of CMCs are essential for diagnosis and prognosis of the cancer. Existing techniques (such as immune-mediated assays and polymerase chain reaction) for CMC detection rely primarily on antigen-antibody recognition or physical properties of tumor cells, and suffer from inadequate sensitivity and specificity due to extremely low levels of CMCs in the blood[52,53].

To address this critical need, multiple PAI studies for CMC detection have been performed. One early-stage study detected melanoma cells in human blood samples from a patient with stage-IV melanoma using a photoacoustic flowmetry system[54]. Muliple photoacoustic flow cytometry (PAFC) systems have been developed to enumerate CMCs in early-stage melanoma patients (I–III stages), showing a capability of detecting 2 CMCs/ml in human blood draws. Out of 27 patients (67%) with more than two CMCs/ml detected by the PAFC, 18 eventually developed metastatic diseases during their follow-up times[52]. In another study, a cytophone PAFC system was invented which detected CMCs in 27 of 28 of melanoma patients, yet reported zero CMC events in healthy participants[55]. Recently, a linear array-based PACT system has been optimized for the detection of CMCs subcutaneously in stage III-IV melanoma patients in vivo. Patients with positive test results had higher chances of disease progression in follow-up studies[56].

Moreover, PAFC holds promise for improving the prevention of metastatic disease through the targeted elimination of melanoma cells in circulation. A dual-wavelength PAFC has been developed, integrated with a melanoma-specific laser therapy mechanism[57]. The in-vivo label-free imaging of CMCs in mice enabled the immediate initiation of a targeted laser treatment upon detection of the melanoma cell's photoacoustic signal. The melanoma cell was thermally destroyed without collateral damage[57].

3.1.3. Non-invasive Tumor Margin Imaging of Non-melanoma

Different from melanoma, non-melanoma skin cancers (NMSCs) typically exhibit less aggressiveness and lower metastatic tendencies, underscoring the crucialness of complete surgical excision[58]. However, accurate measurement of tumor size is critical for successful tumor resection. Accordingly, preoperative imaging is helpful to improve precise excisions by providing volumetric information about the melanin concentration and blood vasculature. Non-invasive preoperative imaging also aids in the delineation of tumor margins, minimizing the chance of incomplete excision.

 doi:10.20944/preprints202401.1651.v1

This imaging approach aligns seamlessly with Mohs surgery to shortening the operative procedures and improve the cost effectiveness[59].

NMSCs are often lightly pigmented and contain melanin, serving as an endogenous contrast agent for PAI. A recent study successfully distinguished NMSC tumors from normal skin in 21 Asian NMSC patients imaged by MSOT (Multispectral Optoacoustic Tomography), which analyzed the optical spectrum of the lesion (Figure 1(e))[31]. Its real-time 3D imaging capability also allowed visualization of the lesion's structures and associated vascular angiogenesis, which is a well-acknowledged indication of tumor invasiveness[60,61]. Another approach involves a planar-view PACT using a Fabry-Pérot interferometer (FPI) to provide higher acoustic detection performance than piezoelectric transducers[62]. The transparent FPI sensor also facilitates integration with other optical imaging modalities, such as OCT[63]. Proof-of-principle studies have demonstrated 3D imaging of a surgical scar and basal cell carcinoma in human skin. In addition to the anatomical imaging of NMSC-associated angiogenesis, multi-spectral PAI is capable of mapping oxygen saturation in tumor microenviroments to identify hypoxia-related malignancy biomarkers[64].

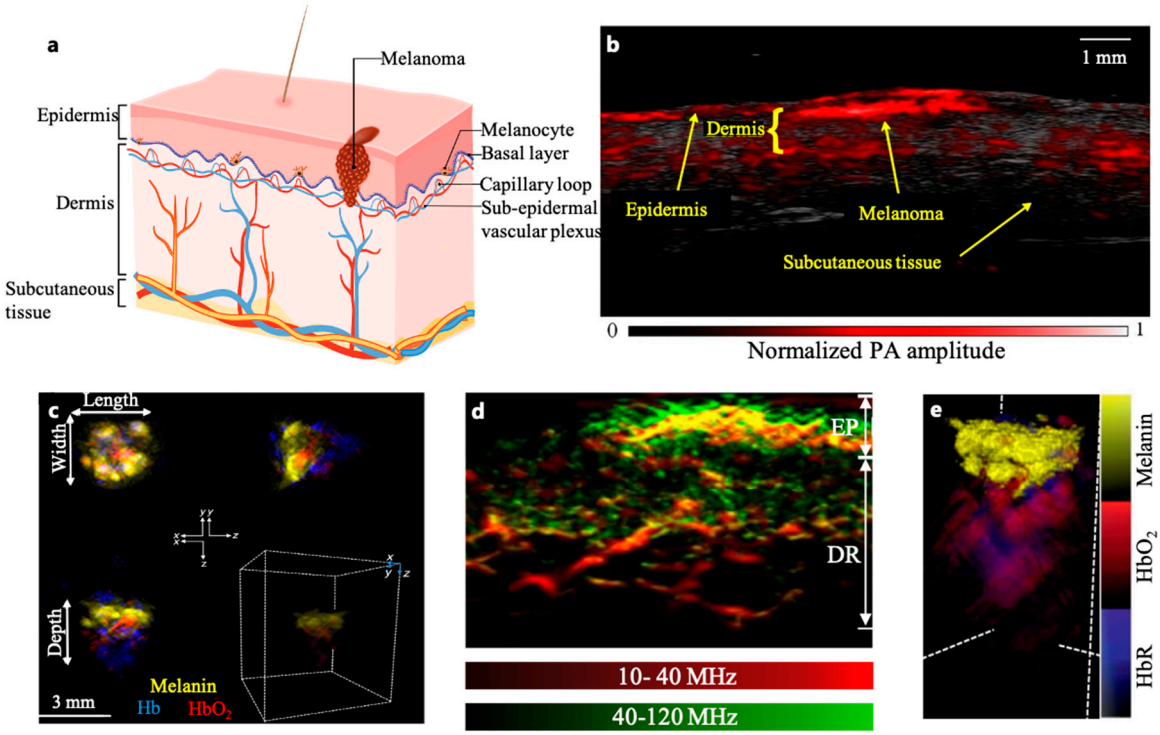

Figure 1. (a) Layers of human skin. (b) Coregistered PAI image of in situ melanoma on upper left extremity. Handheld linear-array-based PAI was able to image pigmented lesion and skin architecture with high contrast, speed, and resolution[42]. (c) In vivo Volumetric Multispectral optoacoustic tomography(vMSOT) images in different orthogonal views and 3D map of skin tumour showing melanin, Hb (blue) and HbO_2 (red) signals. Clusters of melanin signals were observed with strong haemoglobin signals underneath the tumour, indicating the extent of tumour's vascularity. Measurements of tumour dimensions were acquired from the xy and xz planes to get the maximum length, width and depth (including vasculature) parameters[44]. (d) Maximum intensity projection (MIP) cross-sectional images of a melanoma lesion edge (red: larger structures in the bandwidth of 10–40 MHz; green: smaller structures in the bandwidth of 40–120 MHz) [46]. (e) 3D MSOT rendering of a representative BCC lesion showing melanin (yellow), Hb (blue) and HbO_2 (red) signals. Melanin signals were clustered at the top with strong hemoglobin signals underneath the BCC, showing deeper vasculature structures and the lesion[31].

 doi:10.20944/preprints202401.1651.v1

3.2. Psoriasis

Psoriasis is a chronic skin disease mainly characterized by the appearance of abnormal skin patches[65,66]. Histology of psoriatic skin exhibits hyperkeratosis, acanthosis, inflammatory cellular infiltrate, and modified microvascular architecture (Figure 2(a)). Clinics typically evaluate psoriasis via visual assessment based on the Psoriasis Area and Severity Index (PASI) scoring system. Although diagnostic accuracy is limited by the lack of subcutaneous information and by subjective judgment, the evolving understanding of this disease has made microvascular alterations become crucial pathophysiological markers in the objective assessment of psoriasis progression[67,68].

Studies have successfully demonstrated PAI of microvascular lesions in psoriasis, providing a valuable approach to identify and quantitatively measure specific biomarkers for early screening and accurate diagnosis. The PAI of psoriasis biomarkers include elongated and dilated capillary loops as well as dermal vessels with larger diameters and denser distributions than those in healthy skin (Figure 2(b)(c))[46,69]. For example, using raster-scan optoacoustic mesoscopy (RSOM) (Figure 2(d)(e)), PAI studies have revealed correlations between microvascular characteristics and psoriasis response to treatment. Characteristics such as the mean capillary loop length, mean capillary loop diameter, and mean width (thickness) of the sub-epidermal vascular plexus have shown strong associations with treatment outcomes (r^2= 0.77, P = 0.00004)[70]. These parameters can be effectively monitored by PAI to capture the therapeutic responses that may elude conventional PASI evaluation[70]. The combination of PAI and OCT has proved mutual corroboration with different scales and depths in dermatitis images[69,71].

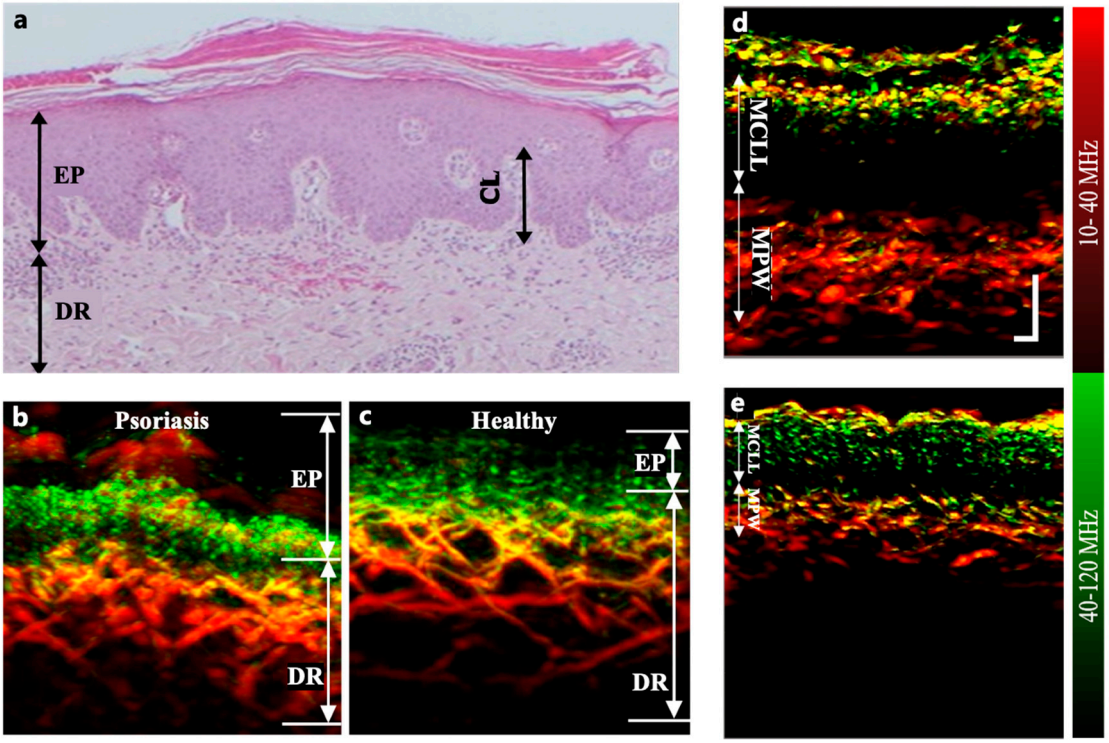

Figure 2. (a) Histological cross section of psoriatic skin showing acanthosis, hyperkeratosis, and elongated capillary loop (CL)[70]. The sub-epidermal vascular plexus appears dilated. (b)and(c) Cross-sectional MIP images of psoriatic skin and adjacent healthy skin from a patient's back (male)[46]. (d)and(e) Coronal RSOM images of the same psoriatic plaque on days 1 and 10 of conventional treatment with the PASI 7 and 2 . All photoacoustic images are color-coded to represent the two reconstructed frequency bands (red: larger structures in the bandwidth of 10–40 MHz; green: smaller structures in the bandwidth of 40–120 MHz)[70].

 doi:10.20944/preprints202401.1651.v1

3.3. PAI of Some Other Skin Diseases

The imaging of subcutaneous blood oxygen saturation holds significant diagnostic value in hypoxia-associated conditions such as systemic sclerosis and vascular malformations. Systemic sclerosis, characterized by skin fibrosis and progressive vascular involvement, relies primarily on nailfold capillaroscopy for diagnosis[72]. However, superficial nailfold microvasculature cannot fully represent epidermal conditions. Therefore, RSOM has been used to generate three-dimensional images of the entire nailfold microvascular network that includes dermal vessels (Figure 3(a))[73,74]. Multispectral PAI, which is emerging as an important tool for imaging vascular malformations, has also revealed an abnormal increase in arterial blood oxygen saturation (SaO2) within arteriovenous malformations. Such pathological image features allow PAI to provide crucial insights that may benefit invidualized therapy (Figure 3(b))[75].

Diabetes is condition which affects the microvasculature of various organs, including the eyes, heart, brain, kidneys, and skin[76,77]. The skin is the most accessible organ and could offer a window for detecting diabetes-related systemic effects on the microvasculature. In a study involving 72 diabetic patients, RSOM was employed to image the lower limbs, and six label-free optoacoustic biomarkers were extracted (Figure 3(c))[78–80]. The effects of diabetes on these parameters were investigated as a function of disease severity, finding strong statistically significant differences between microvasculature parameters and diabetes progression. Alterations induced by diabetes in the microvasculature of the skin serve as indicative markers of an unfavorable disease prognosis. These alterations compromise tissue perfusion and oxygenation, as well as the integrity of skin barriers, thereby predisposing individuals to cutaneous infections, neuropathy characterized by sensory loss, ulcerations, and other associated comorbidities such as diabetic foot ulcers [81,82]. PAI holds promise as an effective tool for early detection, potentially transforming the prognosis for this condition[80,83].

Moreover, diabetic foot ulcers are a common and severe complication of type 2 diabetes mellitus, with the potential risk of amputation and even life-threatening consequences arising from persistent ulcers or associated infections[84]. The occurrence of diabetic foot ulcers is intricately linked to microcirculation in the foot, a result of the collective impact of diabetic lower limb neuropathy or peripheral vasculopathy[85]. The dermal vascular system, situated beneath the highly scattering epidermis, remains inaccessible through optical microscopy methods such as confocal or two-photon microscopy. Conventional approaches like ultrasound encounter challenges in visualizing microvessels below the ankle, limiting the assessment of foot microcirculation and impeding the detection of microangiopathy in diabetic foot ulcer patients. PAI, combining the advantages of optical and acoustic techniques with higher resolution and penetration depth, provides a clear observation of the dermal vascular network. He et al. utilized ROSM for skin imaging of the lower extremities in diabetic participants, resolving skin vessels with diameters ranging from 10 μm to about 150 μm[79]. This capability facilitates quantitative research on biomarkers associated with neuropathy and peripheral vasculopathy. With the progression of diabetes, a reduction in vascular density in the dermal layer and thinning of the epidermis are observed. The high resolution and penetration depth of PAI therefore paves the way for an in-depth exploration of micro-vascular changes relevant to the pathology of diabetic foot ulcers, providing valuable insights for early diagnosis, treatment planning, and preventive strategies.

The potential application landscape of PAI in systemic lupus erythematosus (SLE) is expansive. This imaging modality has proven its value in examining the vasculature[31,46], joints[86,87], and skin injuries[31,43,88], providing a range of insights into the depth and breadth of vascular structural abnormalities, arthritic inflammation, and skin damage. Given the autoimmune nature of SLE, characterized by vascular inflammation similar to psoriasis, PAI assists in observing changes in vascular structure. SLE often presents with joint inflammation, and PAI allows for non-invasive observation of joint structure and inflammation, facilitating early detection and continuous monitoring of disease activity. Furthermore, SLE typically manifests as skin damage, including erythema and ulcers. PAI, with its high-resolution capabilities, provides detailed skin images, assisting physicians in observing the depth and extent of skin lesions. This not only aids in early

 doi:10.20944/preprints202401.1651.v1

detection but also enables more accurate monitoring of pathological changes in SLE, thereby offering robust support for physicians in developing personalized treatment plans. Although PAI is still in the research phase within the lupus erythematosus domain, its unique advantages position it as a powerful tool for future in-depth understanding of autoimmune diseases.

In addition, using only hemoglobin and water as the endogenous contrast, PAI has the potential to characterize the pathological features of healthy skin, superficial dermal burns, deep dermal burns, and deep burns[89]. For acute burns, PAI can clearly delineate the hyperemic bowl, the boundary between the edemic coagulated burned tissue and the healthy perfused tissue (Figure 3(d))[88]. To mitigate the risk of infection and eliminate direct contact with injured skin, non-contact PAI methods have been developed, such as non-contact photoacoustic imaging with focused air-coupled transducers and non-contact photoacoustic imaging using fiber-based interferometers, showing substantial application potential[90,91]. However, non-contact photoacoustic imaging faces challenges related to reduced signal sensitivity. The necessity for the signal to travel through air or other media may introduce signal attenuation, impacting the imaging sensitivity. Additionally, certain non-contact photoacoustic imaging methods may face limitations concerning the distance the signal travels, particularly when imaging deep tissues. This limitation can lead to lower resolution in deep tissues compared to direct contact methods.

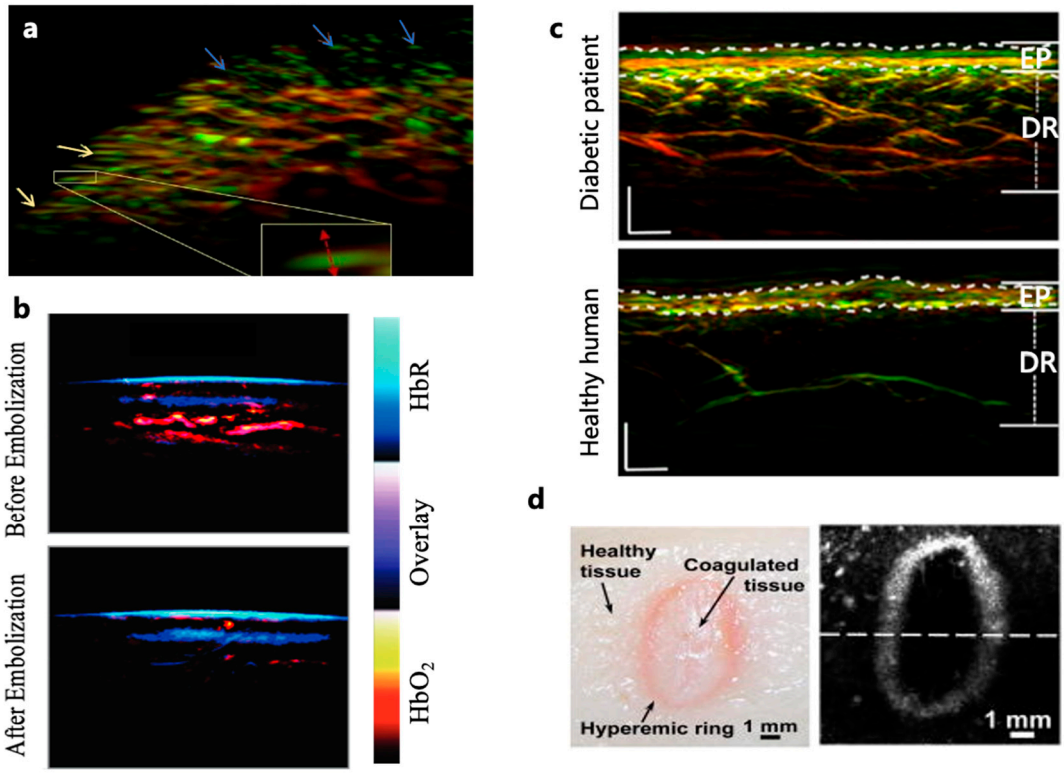

Figure 3 (a) Three dimensional imaging of the nailfold microvasculature. Yellow arrows indicate capillaries close to the nail; blue arrows show capillaries further from the nail tend to orient perpendicular to the skin[73]. (b) Pseudocolor-coded MSOT skin images, showing reduced HbO_2 concentration after complete arteriovenous malformation embolization treatment[75]. (c) PAI of lower extremities (distal pretibial region), showing noticeable difference between healthy subjects and diabetitc patients [78]. (d) Photograph and AR-PAM image of an acute skin burn induced by 175 °C heat exposure for 20 seconds, showing the characteristic hyperemic ring[88].

4. Conclusion and Perspective

This review highlights the potential of PAI as a transformative tool for accurate diagnosis and treatment guidance in dermatology. The distinct absorption spectra of biological components acquired by PAI enable visualization of a wide range of endogenous and exogenous absorbers and

provide detailed insights into pathological characteristics. For example, the high imaging contrast of melanin and hemoglobin allows PAI to measure melanoma depth and microvasculature distruction for improved diagnosis. Moreover, PAI can extend to the detection and treatment of circulating melanoma cells, offering a valuable tool for prognosis and personalized treatment. In the context of NMSCs, where accurate measurement of tumor size is critical, PAI shows early promise in accurately distinguishing NMSCs from healthy tissue. In addition to solid tumor imaging, PAI has shown significant benefits in psoriasis diagnosis. Its capability of capturing microvascular alterations in psoriatic skin provides dermatologists a quantitative and objective approach for early screening and accurate diagnosis, offering an improvement over conventional visual assessments. Furthermore, PAI has been demonstrated to measure subcutaneous blood oxygen saturation, offering diagnostic insights into conditions like systemic sclerosis and chronic wounds. Clinical imaging requirement in superficial diseases such as ulcers and diabetes-related lesions further extend the applications of PAI in improving early detection and accurate diagnosis by revealing additional pathological features under the epidermis.

The technical advantages and niche clinical applications of PAI have been clearly demonstrated. However, challenges remain, including imaging standardization across diverse patient populations, and the establishing of regulatory frameworks for system construction and usage. The translation of PAI from a laboratory technology to a clinical product requires ongoing work to improve reliability, develop expert consensus, and establish clinical guidelines. The recent FDA approval of a PAI system for breast cancer diagnosis exemplifies its growing acceptance in clinical practice and paves the way to additional applications. Overall, the unique advantages and continued development of PAI holds great promise for accurate skin disease diagnosis and treatment management.

Author Contributions: Writing—original draft preparation, Y.Y.; writing—review and editing, L.L.; visualization, L.L. and H.Z.; supervision, L.L. and H.Z.; project administration, Y.Y.; funding acquisition, L.L. and H.Z. All authors have read and agreed to the published version of the manuscript.

Funding: This research received no external funding

Conflicts of Interest: The authors declare no conflicts of interest.

References

1. Schneider, S.L.; Kohli, I.; Hamzavi, I.H.; Council, M.L.; Rossi, A.M.; Ozog, D.M. Emerging imaging technologies in dermatology. *Journal of the American Academy of Dermatology* **2019**, *80*, 1114–1120, doi:10.1016/j.jaad.2018.11.042.
2. Marchetti, M.A.; Cowen, E.A.; Kurtansky, N.R.; Weber, J.; Dauscher, M.; DeFazio, J.; Deng, L.; Dusza, S.W.; Haliasos, H.; Halpern, A.C.; et al. Prospective validation of dermoscopy-based open-source artificial intelligence for melanoma diagnosis (PROVE-AI study). *npj Digit. Med.* **2023**, *6*, 127, doi:10.1038/s41746-023-00872-1.
3. Alenezi, F.; Armghan, A.; Polat, K. A multi-stage melanoma recognition framework with deep residual neural network and hyperparameter optimization-based decision support in dermoscopy images. *Expert Systems with Applications* **2023**, *215*, 119352, doi:10.1016/j.eswa.2022.119352.
4. Infante, V.H.; Maia Campos, P. Application of a Reflectance Confocal Microscopy Imaging Analysis Score for the Evaluation of NON-MELANOGENIC Changes in Male Photoaged Skin. *Photochem & Photobiology* **2023**, *99*, 993–1002, doi:10.1111/php.13713.
5. Perino, F.; Suarez, R.; Perez-Anker, J.; Carrera, C.; Rezze, G.G.; Primiero, C.A.; Alos, L.L.; Díaz, A.; Barreiro, A.; Puig, S.; et al. Concordance of in vivo reflectance confocal microscopy and horizontal-sectioning histology in skin tumours. *Acad Dermatol Venereol* **2024**, *38*, 124–135, doi:10.1111/jdv.19491.
6. Cinotti, E.; Brunetti, T.; Cartocci, A.; Tognetti, L.; Suppa, M.; Malvehy, J.; Perez-Anker, J.; Puig, S.; Perrot, J.L.; Rubegni, P. Diagnostic Accuracy of Line-Field Confocal Optical Coherence Tomography for the Diagnosis of Skin Carcinomas. *Diagnostics* **2023**, *13*, 361, doi:10.3390/diagnostics13030361.
7. Kim, H.; Kang, D.; Seong, D.; Saleah, S.A.; Luna, J.A.; Kim, Y.; Kim, H.; Han, S.; Jeon, M.; Kim, J. Skin pore imaging using spectral-domain optical coherence tomography: a case report. *Biomed. Eng. Lett.* **2023**, *13*, 729–737, doi:10.1007/s13534-023-00290-y.
8. Wortsman, X. Top applications of dermatologic ultrasonography that can modify management. *Ultrasonography* **2023**, *42*, 183–202, doi:10.14366/usg.22130.
9. Płocka, M.; Czajkowski, R. High-frequency ultrasound in the diagnosis and treatment of skin neoplasms. *Advances in Dermatology and Allergology*.

10. Alex, A.; Chaney, E.J.; Žurauskas, M.; Criley, J.M.; Spillman Jr., D.R.; Hutchison, P.B.; Li, J.; Marjanovic, M.; Frey, S.; Arp, Z.; et al. In vivo characterization of minipig skin as a model for dermatological research using multiphoton microscopy. *Experimental Dermatology* **2020**, *29*, 953–960, doi:10.1111/exd.14152.
11. Marconi, A.; Quadri, M.; Farnetani, F.; Ciardo, S.; Palazzo, E.; Lotti, R.; Cesinaro, A.M.; Fabbiani, L.; Vaschieri, C.; Puviani, M.; et al. In Vivo Melanoma Cell Morphology Reflects Molecular Signature and Tumor Aggressiveness. *Journal of Investigative Dermatology* **2022**, *142*, 2205-2216.e6, doi:10.1016/j.jid.2021.12.024.
12. Schmid-Wendtner, M.-H.; Dill-Müller, D. Ultrasound Technology in Dermatology. *Seminars in Cutaneous Medicine and Surgery* **2008**, *27*, 44–51, doi:10.1016/j.sder.2008.01.003.
13. Lin, L. High-speed three-dimensional photoacoustic computed tomography for preclinical research and clinical translation. 10.
14. Attia, A.B.E.; Balasundaram, G.; Moothanchery, M.; Dinish, U.S.; Bi, R.; Ntziachristos, V.; Olivo, M. A review of clinical photoacoustic imaging: Current and future trends. *Photoacoustics* **2019**, *16*, 100144, doi:10.1016/j.pacs.2019.100144.
15. Deán-Ben, X.L.; Fehm, T.F.; Ford, S.J.; Gottschalk, S.; Razansky, D. Spiral volumetric optoacoustic tomography visualizes multi-scale dynamics in mice. *Light Sci Appl* **2017**, *6*, e16247–e16247, doi:10.1038/lsa.2016.247.
16. Wang, L.V.; Yao, J. A practical guide to photoacoustic tomography in the life sciences. *Nat Methods* **2016**, *13*, 627–638, doi:10.1038/nmeth.3925.
17. Wang, L.V. Multiscale photoacoustic microscopy and computed tomography. *Nature Photon* **2009**, *3*, 503–509, doi:10.1038/nphoton.2009.157.
18. Wang, L.V.; Hu, S. Photoacoustic Tomography: In Vivo Imaging from Organelles to Organs. *Science* **2012**, *335*, 1458–1462, doi:10.1126/science.1216210.
19. Chen, S.-L.; Guo, L.J.; Wang, X. All-optical photoacoustic microscopy. *Photoacoustics* **2015**, *3*, 143–150, doi:10.1016/j.pacs.2015.11.001.
20. Hu, S.; Maslov, K.; Wang, L.V. Second-generation optical-resolution photoacoustic microscopy with improved sensitivity and speed. *Opt. Lett.* **2011**, *36*, 1134, doi:10.1364/OL.36.001134.
21. Lin, L.; Zhang, P.; Xu, S.; Shi, J.; Li, L.; Yao, J.; Wang, L.; Zou, J.; Wang, L.V. Handheld optical-resolution photoacoustic microscopy. *J. Biomed. Opt* **2016**, *22*, 041002, doi:10.1117/1.JBO.22.4.041002.
22. Favazza, C.P.; Wang, L.V.; Jassim, O.W.; Cornelius, L.A. In vivo photoacoustic microscopy of human cutaneous microvasculature and a nevus. *J. Biomed. Opt.* **2011**, *16*, 1, doi:10.1117/1.3528661.
23. Zhang, H.F.; Maslov, K.; Stoica, G.; Wang, L.V. Functional photoacoustic microscopy for high-resolution and noninvasive in vivo imaging. *Nat Biotechnol* **2006**, *24*, 848–851, doi:10.1038/nbt1220.
24. Yao, J.; Wang, L.V. Photoacoustic microscopy: Photoacoustic microscopy. *Laser & Photonics Reviews* **2013**, *7*, 758–778, doi:10.1002/lpor.201200060.
25. Xia, J.; Yao, J.; Wang, L.V. Photoacoustic tomography: principles and advances. **2015**.
26. Lin, L.; Hu, P.; Shi, J.; Appleton, C.M.; Maslov, K.; Li, L.; Zhang, R.; Wang, L.V. Single-breath-hold photoacoustic computed tomography of the breast. *NATURE COMMUNICATIONS* **2018**, *9*.
27. Yao, J.; Wang, L.; Yang, J.-M.; Maslov, K.I.; Wong, T.T.W.; Li, L.; Huang, C.-H.; Zou, J.; Wang, L.V. High-speed label-free functional photoacoustic microscopy of mouse brain in action. *Nat Methods* **2015**, *12*, 407–410, doi:10.1038/nmeth.3336.
28. Lin, L.; Yao, J.; Zhang, R.; Chen, C.; Huang, C.; Li, Y.; Wang, L.; Chapman, W.; Zou, J.; Wang, L.V. High-speed photoacoustic microscopy of mouse cortical microhemodynamics. *J. Biophoton.* **2017**, *10*, 792–798, doi:10.1002/jbio.201600236.
29. Stein, E.W.; Maslov, K.; Wang, L.V. Noninvasive, in vivo imaging of blood-oxygenation dynamics within the mouse brain using photoacoustic microscopy. *J. Biomed. Opt.* **2009**, *14*, 020502, doi:10.1117/1.3095799.
30. Lan, B.; Liu, W.; Wang, Y.; Shi, J.; Li, Y.; Xu, S.; Sheng, H.; Zhou, Q.; Zou, J.; Hoffmann, U.; et al. High-speed widefield photoacoustic microscopy of small-animal hemodynamics. *Biomed. Opt. Express* **2018**, *9*, 4689, doi:10.1364/BOE.9.004689.
31. Attia, A.B.E.; Chuah, S.Y.; Razansky, D.; Ho, C.J.H.; Malempati, P.; Dinish, U.S.; Bi, R.; Fu, C.Y.; Ford, S.J.; Lee, J.S.-S.; et al. Noninvasive real-time characterization of non-melanoma skin cancers with handheld optoacoustic probes. *Photoacoustics* **2017**, *7*, 20–26, doi:10.1016/j.pacs.2017.05.003.
32. Li, D.; Humayun, L.; Vienneau, E.; Vu, T.; Yao, J. Seeing through the Skin: Photoacoustic Tomography of Skin Vasculature and Beyond. *JID Innovations* **2021**, *1*, 100039, doi:10.1016/j.xjidi.2021.100039.
33. Stoffels, I.; Morscher, S.; Helfrich, I.; Hillen, U.; Leyh, J.; Burton, N.C.; Sardella, T.C.P.; Claussen, J.; Poeppel, T.D.; Bachmann, H.S.; et al. Metastatic status of sentinel lymph nodes in melanoma determined noninvasively with multispectral optoacoustic imaging. *Sci. Transl. Med.* **2015**, *7*, doi:10.1126/scitranslmed.aad1278.
34. Kalaora, S.; Nagler, A.; Wargo, J.A.; Samuels, Y. Mechanisms of immune activation and regulation: lessons from melanoma. *Nat Rev Cancer* **2022**, *22*, 195–207, doi:10.1038/s41568-022-00442-9.

35. Schadendorf, D.; van Akkooi, A.C.J.; Berking, C.; Griewank, K.G.; Gutzmer, R.; Hauschild, A.; Stang, A.; Roesch, A.; Ugurel, S. Melanoma. *The Lancet* **2018**, *392*, 971–984, doi:10.1016/S0140-6736(18)31559-9.
36. US Preventive Services Task Force; Bibbins-Domingo, K.; Grossman, D.C.; Curry, S.J.; Davidson, K.W.; Ebell, M.; Epling, J.W.; García, F.A.R.; Gillman, M.W.; Kemper, A.R.; et al. Screening for Skin Cancer: US Preventive Services Task Force Recommendation Statement. *JAMA* **2016**, *316*, 429, doi:10.1001/jama.2016.8465.
37. Switzer, B.; Puzanov, I.; Skitzki, J.J.; Hamad, L.; Ernstoff, M.S. Managing Metastatic Melanoma in 2022: A Clinical Review. *JCO Oncol Pract* **2022**, *18*, 335–351, doi:10.1200/OP.21.00686.
38. Schadendorf, D.; Fisher, D.E.; Garbe, C.; Gershenwald, J.E.; Grob, J.-J.; Halpern, A.; Herlyn, M.; Marchetti, M.A.; McArthur, G.; Ribas, A.; et al. Melanoma. *Nat Rev Dis Primers* **2015**, *1*, 15003, doi:10.1038/nrdp.2015.3.
39. Kelly, J.W.; Henderson, M.A.; Thursfield, V.J.; Slavin, J.; Ainslie, J.; Giles, G.G. The management of primary cutaneous melanoma in Victoria in 1996 and 2000. *Medical Journal of Australia* **2007**, *187*, 511–514, doi:10.5694/j.1326-5377.2007.tb01392.x.
40. Hieken, T.J.; Hernández-Irizarry, R.; Boll, J.M.; Jones Coleman, J.E. Accuracy of Diagnostic Biopsy for Cutaneous Melanoma: Implications for Surgical Oncologists. *International Journal of Surgical Oncology* **2013**, *2013*, 1–7, doi:10.1155/2013/196493.
41. Ng, J.C.; Swain, S.; Dowling, J.P.; Wolfe, R.; Simpson, P.; Kelly, J.W. The Impact of Partial Biopsy on Histopathologic Diagnosis of Cutaneous Melanoma: Experience of an Australian Tertiary Referral Service. *Archives of Dermatology* **2010**, *146*, 234–239, doi:10.1001/archdermatol.2010.14.
42. Breathnach, A.; Concannon, E.; Dorairaj, J.J.; Shaharan, S.; McGrath, J.; Jose, J.; Kelly, J.L.; Leahy, M.J. Preoperative measurement of cutaneous melanoma and nevi thickness with photoacoustic imaging. *J. Med. Imag.* **2018**, *5*, 1, doi:10.1117/1.JMI.5.1.015004.
43. Zhou, Y.; Tripathi, S.V.; Rosman, I.; Ma, J.; Hai, P.; Linette, G.P.; Council, M.L.; Fields, R.C.; Wang, L.V.; Cornelius, L.A. Noninvasive Determination of Melanoma Depth using a Handheld Photoacoustic Probe. *Journal of Investigative Dermatology* **2017**, *137*, 1370–1372, doi:10.1016/j.jid.2017.01.016.
44. Chuah, S.Y.; Attia, A.B.E.; Long, V.; Ho, C.J.H.; Malempati, P.; Fu, C.Y.; Ford, S.J.; Lee, J.S.S.; Tan, W.P.; Razansky, D.; et al. Structural and functional 3D mapping of skin tumours with non-invasive multispectral optoacoustic tomography. *Skin Res Technol* **2017**, *23*, 221–226, doi:10.1111/srt.12326.
45. Zhou, W.; Chen, Z.; Yang, S.; Xing, D. Optical biopsy approach to basal cell carcinoma and melanoma based on all-optically integrated photoacoustic and optical coherence tomography. *Opt. Lett.* **2017**, *42*, 2145, doi:10.1364/OL.42.002145.
46. He, H.; Schönmann, C.; Schwarz, M.; Hindelang, B.; Berezhnoi, A.; Steimle-Grauer, S.A.; Darsow, U.; Aguirre, J.; Ntziachristos, V. Fast raster-scan optoacoustic mesoscopy enables assessment of human melanoma microvasculature in vivo. *Nat Commun* **2022**, *13*, 2803, doi:10.1038/s41467-022-30471-9.
47. Zhou, W.; Chen, Z.; Zhou, Q.; Xing, D. Optical Biopsy of Melanoma and Basal Cell Carcinoma Progression by Noncontact Photoacoustic and Optical Coherence Tomography: *In Vivo* Multi-Parametric Characterizing Tumor Microenvironment. *IEEE Trans. Med. Imaging* **2020**, *39*, 1967–1974, doi:10.1109/TMI.2019.2962614.
48. Omar, M.; Schwarz, M.; Soliman, D.; Symvoulidis, P.; Ntziachristos, V. Pushing the Optical Imaging Limits of Cancer with Multi-Frequency-Band Raster-Scan Optoacoustic Mesoscopy (RSOM). *Neoplasia* **2015**, *17*, 208–214, doi:10.1016/j.neo.2014.12.010.
49. Massagué, J.; Obenauf, A.C. Metastatic colonization by circulating tumour cells. *Nature* **2016**, *529*, 298–306, doi:10.1038/nature17038.
50. Fidler, I.J. The pathogenesis of cancer metastasis: the “seed and soil” hypothesis revisited. *Nat Rev Cancer* **2003**, *3*, 453–458, doi:10.1038/nrc1098.
51. Cristofanilli, M.; Budd, G.T.; Ellis, M.J.; Stopeck, A.; Matera, J.; Miller, M.C.; Reuben, J.M.; Doyle, G.V.; Allard, W.J.; Terstappen, L.W.M.M.; et al. Circulating Tumor Cells, Disease Progression, and Survival in Metastatic Breast Cancer. *New England Journal of Medicine* **2004**, *351*, 781–791, doi:10.1056/NEJMoa040766.
52. Edgar, R.H.; Tarhini, A.; Sander, C.; Sanders, M.E.; Cook, J.L.; Viator, J.A. Predicting Metastasis in Melanoma by Enumerating Circulating Tumor Cells Using Photoacoustic Flow Cytometry. *Lasers in Surgery and Medicine* **2021**, *53*, 578–586, doi:10.1002/lsm.23286.
53. Shoji, Y.; Bustos, M.A.; Gross, R.; Hoon, D.S.B. Recent Developments of Circulating Tumor Cell Analysis for Monitoring Cutaneous Melanoma Patients. *Cancers* **2022**, *14*, 859, doi:10.3390/cancers14040859.
54. Weight, R.M.; Dale, P.S.; Viator, J.A. Detection of circulating melanoma cells in human blood using photoacoustic flowmetry. In Proceedings of the 2009 Annual International Conference of the IEEE Engineering in Medicine and Biology Society; 2009; pp. 106–109.
55. Galanzha, E.I.; Menyaev, Y.A.; Yadem, A.C.; Sarimollaoglu, M.; Juratli, M.A.; Nedosekin, D.A.; Foster, S.R.; Jamshidi-Parsian, A.; Siegel, E.R.; Makhoul, I.; et al. In vivo liquid biopsy using Cytophone platform for photoacoustic detection of circulating tumor cells in patients with melanoma. *Science Translational Medicine* **2019**, *11*, eaat5857, doi:10.1126/scitranslmed.aat5857.

56. Hai, P.; Qu, Y.; Li, Y.; Zhu, L.; Shmuylovich, L.; Cornelius, L.A.; Wang, L.V. Label-free high-throughput photoacoustic tomography of suspected circulating melanoma tumor cells in patients in vivo. *J. Biomed. Opt.* **2020**, *25*, 1, doi:10.1117/1.JBO.25.3.036002.
57. He, Y.; Wang, L.; Shi, J.; Yao, J.; Li, L.; Zhang, R.; Huang, C.-H.; Zou, J.; Wang, L.V. In vivo label-free photoacoustic flow cytography and on-the-spot laser killing of single circulating melanoma cells. *Sci Rep* **2016**, *6*, 39616, doi:10.1038/srep39616.
58. Watts, C.; Price, S.J.; Santarius, T. Current Concepts in the Surgical Management of Glioma Patients. *Clinical Oncology* **2014**, *26*, 385–394, doi:10.1016/j.clon.2014.04.001.
59. Etzkorn, J.R.; Alam, M. What Is Mohs Surgery? *JAMA Dermatol* **2020**, *156*, 716, doi:10.1001/jamadermatol.2020.0039.
60. Folkman, J. Angiogenesis in cancer, vascular, rheumatoid and other disease. *Nat Med* **1995**, *1*, 27–30, doi:10.1038/nm0195-27.
61. Carmeliet, P.; Jain, R.K. Angiogenesis in cancer and other diseases. *Nature* **2000**, *407*, 249–257, doi:10.1038/35025220.
62. Plumb, A.A.; Huynh, N.T.; Guggenheim, J.; Zhang, E.; Beard, P. Rapid volumetric photoacoustic tomographic imaging with a Fabry-Perot ultrasound sensor depicts peripheral arteries and microvascular vasomotor responses to thermal stimuli. *Eur Radiol* **2018**, *28*, 1037–1045, doi:10.1007/s00330-017-5080-9.
63. Chen, Z.; Rank, E.; Meiburger, K.M.; Sinz, C.; Hodul, A.; Zhang, E.; Hoover, E.; Minneman, M.; Ensher, J.; Beard, P.C.; et al. Non-invasive multimodal optical coherence and photoacoustic tomography for human skin imaging. *Sci Rep* **2017**, *7*, 17975, doi:10.1038/s41598-017-18331-9.
64. Ron, A.; Deán-Ben, X.L.; Gottschalk, S.; Razansky, D. Volumetric Optoacoustic Imaging Unveils High-Resolution Patterns of Acute and Cyclic Hypoxia in a Murine Model of Breast Cancer. *Cancer Research* **2019**, *79*, 4767–4775, doi:10.1158/0008-5472.CAN-18-3769.
65. Greb, J.E.; Goldminz, A.M.; Elder, J.T.; Lebwohl, M.G.; Gladman, D.D.; Wu, J.J.; Mehta, N.N.; Finlay, A.Y.; Gottlieb, A.B. Psoriasis. *Nat Rev Dis Primers* **2016**, *2*, 16082, doi:10.1038/nrdp.2016.82.
66. Branisteanu, D.E.; Cojocaru, C.; Diaconu, R.; Porumb, E.A.; Alexa, A.I.; Nicolescu, A.C.; Brihan, I.; Bogdanici, C.M.; Branisteanu, G.; Dimitriu, A.; et al. Update on the etiopathogenesis of psoriasis (Review). *Experimental and Therapeutic Medicine* **2022**, *23*, 1–13, doi:10.3892/etm.2022.11124.
67. Griffiths, C.E.; Barker, J.N. Pathogenesis and clinical features of psoriasis. *The Lancet* **2007**, *370*, 263–271, doi:10.1016/S0140-6736(07)61128-3.
68. Ryan, C.; Korman, N.J.; Gelfand, J.M.; Lim, H.W.; Elmets, C.A.; Feldman, S.R.; Gottlieb, A.B.; Koo, J.Y.M.; Lebwohl, M.; Leonardi, C.L.; et al. Research gaps in psoriasis: Opportunities for future studies. *Journal of the American Academy of Dermatology* **2014**, *70*, 146–167, doi:10.1016/j.jaad.2013.08.042.
69. Aguirre, J.; Schwarz, M.; Garzorz, N.; Omar, M.; Buehler, A.; Eyerich, K.; Ntziachristos, V. Precision assessment of label-free psoriasis biomarkers with ultra-broadband optoacoustic mesoscopy. *Nat Biomed Eng* **2017**, *1*, 1–8, doi:10.1038/s41551-017-0068.
70. Hindelang, B.; Nau, T.; Englert, L.; Berezhnoi, A.; Lauffer, F.; Darsow, U.; Biedermann, T.; Eyerich, K.; Aguirre, J.; Ntziachristos, V. Enabling precision monitoring of psoriasis treatment by optoacoustic mesoscopy. *Sci. Transl. Med.* **2022**, *14*, eabm8059, doi:10.1126/scitranslmed.abm8059.
71. Ossadnik, K.; Philipp, S.; Bost, W.; Fournelle, M.; Richter, H.; Lademann, J. Application of Photoacoustic Methods and Confocal Microscopy for Monitoring of Therapeutic Response in Plaque Psoriasis. *Skin Pharmacol Physiol* **2018**, *31*, 308–315, doi:10.1159/000492474.
72. Hindelang, B.; Aguirre, J.; Schwarz, M.; Berezhnoi, A.; Eyerich, K.; Ntziachristos, V.; Biedermann, T.; Darsow, U. Non-invasive imaging in dermatology and the unique potential of raster-scan optoacoustic mesoscopy. *Journal of the European Academy of Dermatology and Venereology* **2019**, *33*, 1051–1061, doi:10.1111/jdv.15342.
73. Aguirre, J.; Hindelang, B.; Berezhnoi, A.; Darsow, U.; Lauffer, F.; Eyerich, K.; Biedermann, T.; Ntziachristos, V. Assessing nailfold microvascular structure with ultra-wideband raster-scan optoacoustic mesoscopy. *Photoacoustics* **2018**, *10*, 31–37, doi:10.1016/j.pacs.2018.02.002.
74. Hofstee, H.M.A.; Serné, E.H.; Roberts, C.; Hesselstrand, R.; Scheja, A.; Moore, T.L.; Wildt, M.; Manning, J.B.; Vonk Noordegraaf, A.; Voskuyl, A.E.; et al. A multicentre study on the reliability of qualitative and quantitative nail-fold videocapillaroscopy assessment. *Rheumatology* **2012**, *51*, 749–755, doi:10.1093/rheumatology/ker403.
75. Masthoff, M.; Helfen, A.; Claussen, J.; Karlas, A.; Markwardt, N.A.; Ntziachristos, V.; Eisenblätter, M.; Wildgruber, M. Use of Multispectral Optoacoustic Tomography to Diagnose Vascular Malformations. *JAMA Dermatology* **2018**, *154*, 1457, doi:10.1001/jamadermatol.2018.3269.
76. Barrett, E.J.; Liu, Z.; Khamaisi, M.; King, G.L.; Klein, R.; Klein, B.E.K.; Hughes, T.M.; Craft, S.; Freedman, B.I.; Bowden, D.W.; et al. Diabetic Microvascular Disease: An Endocrine Society Scientific Statement. *The Journal of Clinical Endocrinology & Metabolism* **2017**, *102*, 4343–4410, doi:10.1210/jc.2017-01922.

77. Cheung, C.Y.; Ikram, M.K.; Klein, R.; Wong, T.Y. The clinical implications of recent studies on the structure and function of the retinal microvasculature in diabetes. *Diabetologia* **2015**, *58*, 871–885, doi:10.1007/s00125-015-3511-1.
78. He, H.; Fasoula, N.-A.; Karlas, A.; Omar, M.; Aguirre, J.; Lutz, J.; Kallmayer, M.; Füchtenbusch, M.; Eckstein, H.-H.; Ziegler, A.-G.; et al. *Optoacoustic skin mesoscopy opens a window to systemic effects of diabetes*; Endocrinology (including Diabetes Mellitus and Metabolic Disease), 2020;
79. He, H.; Fasoula, N.-A.; Karlas, A.; Omar, M.; Aguirre, J.; Lutz, J.; Kallmayer, M.; Füchtenbusch, M.; Eckstein, H.-H.; Ziegler, A.; et al. Opening a window to skin biomarkers for diabetes stage with optoacoustic mesoscopy. *Light Sci Appl* **2023**, *12*, 231, doi:10.1038/s41377-023-01275-3.
80. Karlas, A.; Katsouli, N.; Fasoula, N.-A.; Bariotakis, M.; Chlis, N.-K.; Omar, M.; He, H.; Iakovakis, D.; Schäffer, C.; Kallmayer, M.; et al. Dermal features derived from optoacoustic tomograms via machine learning correlate microangiopathy phenotypes with diabetes stage. *Nat. Biomed. Eng* **2023**, *7*, 1667–1682, doi:10.1038/s41551-023-01151-w.
81. Greenman, R.L.; Panasyuk, S.; Wang, X.; Lyons, T.E.; Dinh, T.; Longoria, L.; Giurini, J.M.; Freeman, J.; Khaodhiar, L.; Veves, A. Early changes in the skin microcirculation and muscle metabolism of the diabetic foot. *The Lancet* **2005**, *366*, 1711–1717, doi:10.1016/S0140-6736(05)67696-9.
82. Caballero, A.E.; Arora, S.; Saouaf, R.; Lim, S.C.; Smakowski, P.; Park, J.Y.; King, G.L.; LoGerfo, F.W.; Horton, E.S.; Veves, A. Microvascular and macrovascular reactivity is reduced in subjects at risk for type 2 diabetes. *Diabetes* **1999**, *48*, 1856–1862, doi:10.2337/diabetes.48.9.1856.
83. Mennes, O.A.; van Netten, J.J.; Slart, R.H.J.A.; Steenbergen, W. Novel Optical Techniques for Imaging Microcirculation in the Diabetic Foot. *CPD* **2018**, *24*, 1304–1316, doi:10.2174/1381612824666180302141902.
84. McDermott, K.; Fang, M.; Boulton, A.J.M.; Selvin, E.; Hicks, C.W. Etiology, Epidemiology, and Disparities in the Burden of Diabetic Foot Ulcers. *Diabetes Care* **2023**, *46*, 209–221, doi:10.2337/dci22-0043.
85. Huang, F.; Lu, X.; Yang, Y.; Yang, Y.; Li, Y.; Kuai, L.; Li, B.; Dong, H.; Shi, J. Microenvironment-Based Diabetic Foot Ulcer Nanomedicine. *Advanced Science* **2023**, *10*, 2203308, doi:10.1002/advs.202203308.
86. Wang, Z.; Tong, Z.; Chen, H.; Nie, G.; Hu, J.; Liu, W.; Wang, E.; Yuan, B.; Wang, Z.; Hu, J. Photoacoustic/ultrasonic dual-mode imaging for monitoring angiogenesis and synovial erosion in rheumatoid arthritis. *Photoacoustics* **2023**, *29*, 100458, doi:10.1016/j.pacs.2023.100458.
87. Peng, X.; Xu, Z.; Dentinger, A.; Kewalramani, S.; Jo, J.; Xu, G.; Chamberland, D.; Abdulaziz, N.; Gandikota, G.; Mills, D.; et al. Longitudinal volumetric assessment of inflammatory arthritis via photoacoustic imaging and Doppler ultrasound imaging. *Photoacoustics* **2023**, *31*, 100514, doi:10.1016/j.pacs.2023.100514.
88. Zhang, H.F.; Maslov, K.; D.v.m, G.S.; Wang, L.V. Imaging acute thermal burns by photoacoustic microscopy. *JBO* **2006**, *11*, 054033, doi:10.1117/1.2355667.
89. Yamazaki, M.; Sato, S.; Ashida, H.; Saito, D.; Okada, Y.; Obara, M. Measurement of burn depths in rats using multiwavelength photoacoustic depth profiling. *JBO* **2005**, *10*, 064011, doi:10.1117/1.2137287.
90. Hochreiner, A.; Bauer-Marschallinger, J.; Burgholzer, P.; Jakoby, B.; Berer, T. Non-contact photoacoustic imaging using a fiber based interferometer with optical amplification. *Biomed Opt Express* **2013**, *4*, 2322–2331, doi:10.1364/BOE.4.002322.
91. Deán-Ben, X.L.; Pang, G.A.; Montero de Espinosa, F.; Razansky, D. Non-contact optoacoustic imaging with focused air-coupled transducers. *Appl. Phys. Lett.* **2015**, *107*, 051105, doi:10.1063/1.4928123.